ACS APPLIED MATERIALS & INTERFACES

Research Article

Cite This: ACS Appl. Mater. Interfaces 2019, 11, 10810−10817

www.acsami.org

Highly Conductive Graphene Paper with Vertically Aligned Reduced Graphene Oxide Sheets Fabricated by Improved Electrospray Deposition Technique

Jun-Xiang Yan,[†] Yu-Chen Leng,[‡] Ya-Nan Guo,[†] Guo-Qiang Wang,[§] He Gong,[†] Pei-Zhi Guo,[§] Ping-Heng Tan,[‡] Yun-Ze Long,[†] Xue-Lu Liu,*[,‡] and Wen-Peng Han*[,†]

[†]College of Physics and [§]Institute of Energy & Environmental Materials, School of Materials Science & Engineering, Qingdao University, Qingdao 266071, China

[‡]State Key Laboratory of Superlattices and Microstructures, Institute of Semiconductors, Chinese Academy of Sciences, Beijing 100083, China

Supporting Information

ABSTRACT: Because of its notable electrical and mechanical properties, the highly conductive graphene paper has great potential applications in future flexible electronics. In this study, we report a simple and effective method to prepare vertically aligned graphene oxide papers from graphene oxide suspensions by an improved electrospray deposition technique with a moving stage, which is controlled by computer. Then, the flexible reduced graphene oxide papers are successfully synthesized after reduction by using hydroiodic acid. The obtained reduced graphene oxide paper has an electrical conductivity as high as 6180 S/m, which is more than one and a half times of the reduced graphene oxide paper film, which was fabricated by using the electrospray deposition technique without the moving stage. The experimental results approved for the first time that the degree of alignment of reduced graphene oxide sheets can affect the conductivity of the reduced graphene oxide papers. Further electrochemical measurements for a symmetrical supercapacitor device based on the prepared reduced graphene oxide paper indicate that it has great capacitive performance and electrochemical stability. It exhibited relatively high specific capacitance (174 $F \cdot g^{-1}$) at a current density of 1 $A \cdot g^{-1}$ in 6 M KOH aqueous solution, and its capacitance can retain approximately 86% after 1000 cycles. In addition, patterned freestanding reduced graphene oxide papers, which have potential applications in many fields such as stretchable electronics and wearable devices, also can be fabricated by using this method.

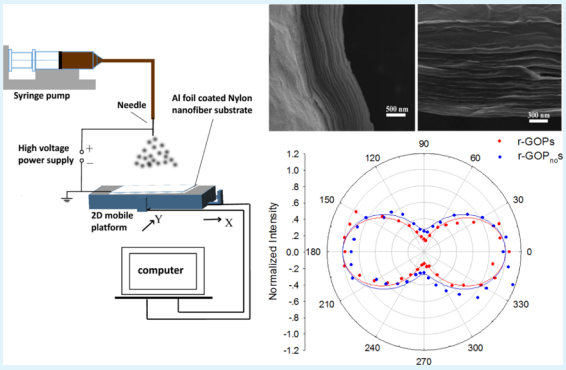

KEYWORDS: *reduced graphene oxide paper, electrospray deposition technique, vertically aligned, high conductivity, stretchable electronics*

1. INTRODUCTION

Highly conductive graphene-based papers, which preserve plenty of remarkable properties of graphene, have recently attracted considerable attention because of its potential application in various fields, such as supercapacitors,[1−3] transparent conductors,[4,5] sensors,[6] and so forth. Owing to the high melting point of inorganic graphene, the fluid assembly is the optimized method to fabricate macroscopic-ordered materials. Until now, producing a graphene-based paper from graphene oxide (GO) still is an accessible and low-cost approach because it is suitable for large-scale production and can easily assemble into a film by solution processes such as vacuum filtration,[7−9] spray coating, dip coating,[4,10] wet spinning,[11] chemically engineering approach,[12] or scrape coating method.[13,14] However, the obtained graphene oxide paper (GOP) is almost an insulator because the GO sheets contain with abundant oxygenated functional groups on their basal plane and edges.[5−16] Therefore, an effective deoxygenating process must be implemented primarily to make the as-prepared insulating GOPs to be conductive. So far, many methods for the reduction of GOPs have been studied including high-temperature thermal annealing[4,17] and low temperature chemical reduction.[5,9,12−14,18−20] These deoxygenating processes are successful for improving the conductivity of the reduced GOPs (r-GOPs). Among them, some representative works have been cited thousands of times by other authors in scientific publications.[4,5,9,18,19] However, the properties of r-GOPs are related to not only the properties of reduced GO (r-GO) sheets but also the arrangement and degree of alignment of r-GO sheets, especially in electrical conductivity. Nevertheless,

Received: November 11, 2018
Accepted: February 26, 2019
Published: February 26, 2019

DOI: 10.1021/acsami.8b19811
ACS Appl. Mater. Interfaces 2019, 11, 10810−10817

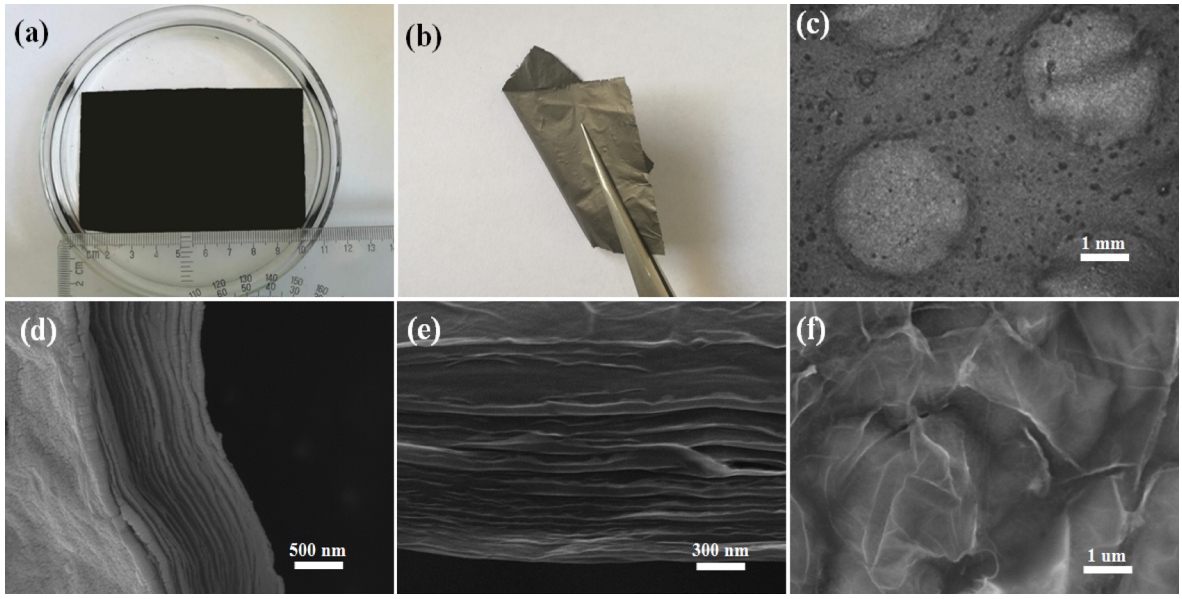

Figure 1. Optical images of (a) GOP with a thickness of 1.2 μm and (b) r-GOP. (c) Optical micrograph of patterned GOP with round holes array. Cross-sectional SEM images of (d) GOP and (e) r-GOP. (f) SEM image of r-GOP (top view).

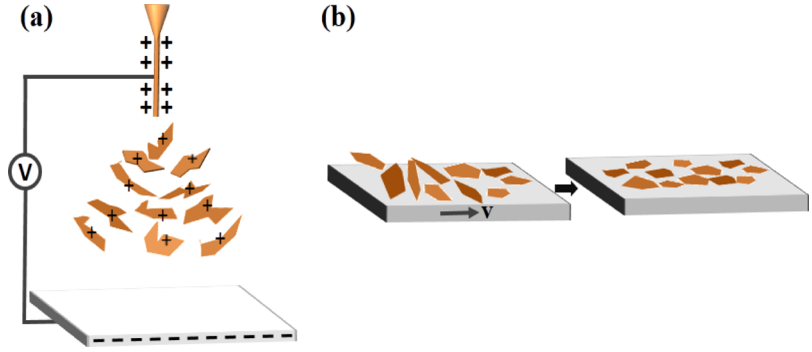

Figure 2. Schematic illustration of the process for fabricating GOPs: (a) the GO sheets in the spraying zone and (b) depositing the GO sheets on the substrate.

those assembly methods mentioned above are difficult to obtain freestanding GOPs with highly vertically aligned GO sheets because of the rigid experimental and process conditions.

As a common fluid assembly technique, electrospray/electrospinning deposition (ESD_spr/ESD_spi) has been widely applied in the fabrication of various thin films because of its high precision for property control and less material loss.[21−25] Recently, because it can effectively improve the uniformity of sheets in the sprayed area, graphene or graphene oxide thin films by the ESD_spr method have been reported and used in a variety of applications, such as resistive switching device,[26] supercapacitor,[1,2] and super thermal management,[27] and so forth. In the ESD_spr process, a precursor solution feeding through a stainless steel nozzle will be atomized at the tip of the nozzle because of the repulsion forces between charges in the droplets after a high electric potential was applied between nozzle and substrate. Then, the atomized small droplets deposit on the substrate to form a uniform thin film. Thus, the properties of the deposition film are closely related to the ESD_spr parameters such as the flow rate of precursor solution, the distance between nozzle and substrate, the applied potential, and so forth.[28] In addition, many studies have demonstrated that the degree of alignment of fibers can be adjusted by changing the relative speed between nozzle and substrate in the ESD_spi process.[29,30] Therefore, the freestanding GOPs with highly vertically aligned GO sheets may be fabricated by using the ESD_spr technology cooperated with a movable substrate.

In this work, we present a more efficient method to prepare vertically aligned GOPs by using an improved ESD_spr technique with a moving stage, which is controlled by computer. After reduction by using hydroiodic acid, the prepared r-GOP film has a higher electrical conductivity more than one and a half times of the r-GOP film, which was fabricated by using the ESD method without a moving stage. For all we know, this is the first time to experimentally prove that the arrangement and degree of alignment of r-GO sheets can affect the conductivity of the r-GOP materials. Further electrochemical measurements for a symmetrical supercapacitor device based on the prepared r-GOP films indicate that it has great capacitive performance. In addition, patterned freestanding r-GOPs, which have potential applications in stretchable electronics and wearable devices, can also be fabricated by using this method.

2. RESULTS AND DISCUSSION

The obtained GOPs and r-GOPs are flexible and freestanding indicating that the individual sheets within the paper have formed continuous networks to provide mechanical integrity

DOI: 10.1021/acsami.8b19811
ACS Appl. Mater. Interfaces 2019, 11, 10810−10817

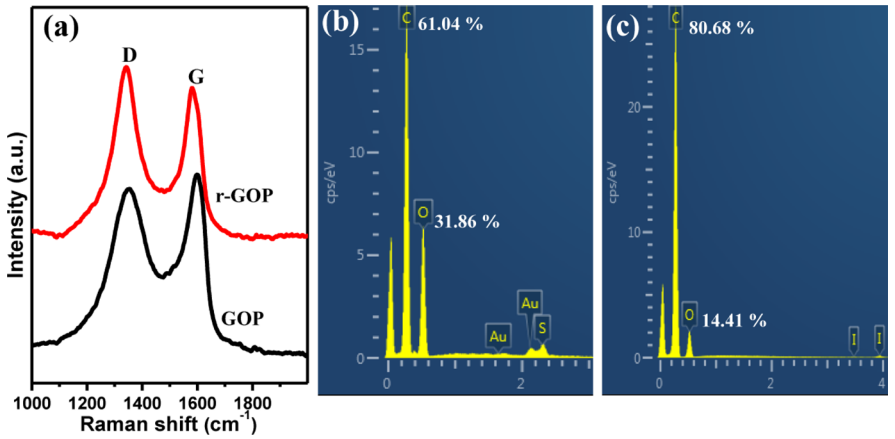

Figure 3. (a) Raman spectra of GOP and r-GOP. Energy dispersive X-ray spectroscopy of (b) GOP and (c) r-GOP.

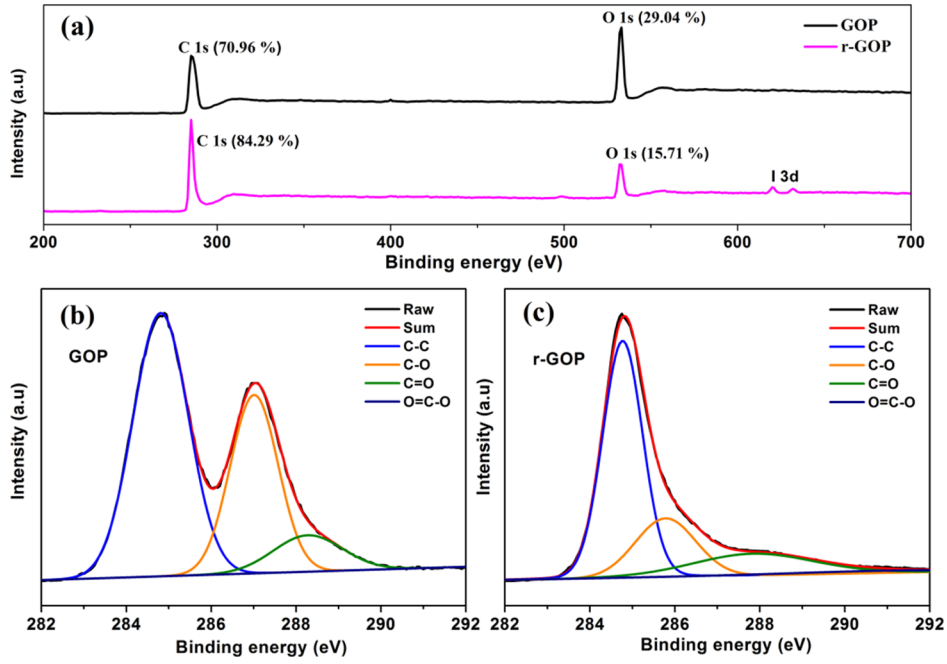

Figure 4. (a) XPS spectra of GOP and r-GOP. XPS C 1s peak of (b) GOP and (c) r-GOP.

and good structure. Photographs of GOP and r-GOP are shown in Figure 1a,b, respectively. The electrical conductivity of the GO sheet has dramatically improved after reduction, which makes the r-GOP film has a metallic luster in comparison to the GOP film, as reported elsewhere.[9,31] Furthermore, patterned freestanding GOPs also can be fabricated by using this setup. The patterned films have potential applications in many fields such as stretchable electronics and wearable devices because they have many advantages in mechanical properties.[32,33] To fabricate the patterned freestanding GOP films, we just need to replace the aluminum foil with the metal substrate with special architectures. Thus, the electric field in the spraying zone can be changed, which can affect the distribution of sediments. For example, the patterned freestanding GOP with a round hole structure, as shown in Figure 1c, was prepared by using the aluminum plate with a round hole array as the collector substrate.

In the synthesis process of the GOP film as shown in Figure 2, the GO sheets were separated in the spraying zone because of the electric field repulsive force and fell toward the collector substrate as a result of the action of electric field attractive force and the gravity of solution as shown in Figure 2a. The GO sheets will bend when they get to the collector substrate because of surface contact stress between them and if the collector substrate keep still or its lateral speed less than the sheet dropping speed. However, once the lateral speed of the collector exceeded the sheet-dropping speed to reach a critical value, the GO sheets will be flat on the collector substrate as shown schematically in Figure 2b. This conclusion comes from the basic knowledge of mechanics and has been proved in the previous study.[29] By carefully adjusting the $ESD_{\_spr}$ parameters such as the flow rate of precursor solution, the distance between nozzle and substrate, the applied potential, and the moving speed of the platform during ESD, a highly vertically aligned structure can be assembled in GOP as shown in Figure 1d. The reduced graphene sheets within the r-GOP film have a looser multilayered structure because of the removal of oxygen-containing functional groups and water molecules intercalated in the spacing between the GO sheets as shown in Figure 1e. In

DOI: 10.1021/acsami.8b19811
ACS Appl. Mater. Interfaces 2019, 11, 10810−10817

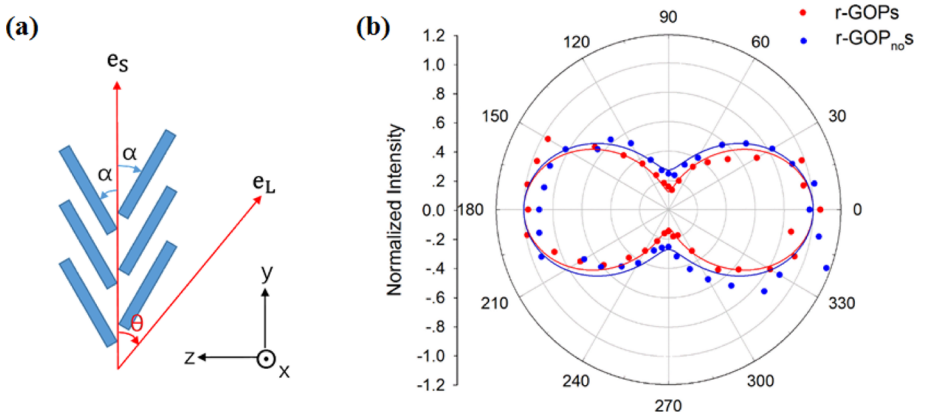

Figure 5. (a) Schematic diagram of simplified model of r-GO sheets and the angle-resolved polarized Raman configuration. (b) Polar plot of the angle-resolved polarized Raman intensity of G mode of r-GOPs and r-GOP$_{no}$s.

addition, the surface of r-GOP still has some protuberant wrinkles and ripples as shown in Figure 1f.

To illustrate the changes in structure and composition after reduction, the structural information and elemental analyses were investigated by Raman, energy dispersive X-ray spectroscopy (EDS), and X-ray photoelectron spectroscopy (XPS). In the Raman spectra of GOP and r-GOP (Figure 3a), they all contain both D and G bands, which are corresponding to the breathing modes of sp^2 atoms and the first-order scattering of the E_{2g} mode, respectively. After reduction, the G band down-shifted to 1582 cm^{-1}, which matched well with that of pristine graphene from 1596 cm^{-1}, and the intensity ratio of two peaks (I_D/I_G) in r-GOP remarkably increased compared to that in GOP, which proves the increase of sp^2 carbon,[34,35] and these all indicating that the GO sheets in GOP were successfully reduced into graphene sheets in r-GOP. In addition, the 2D band (2660 cm^{-1}) (Figure S1) is increased after HI acid reduction, further proves the restoration of sp^2 carbon in r-GOP films.[9,35,42] The increased C/O atomic ratio is another important evidence of the removal of oxygen-containing functional groups of the GO sheets upon reduction.[9] According to the EDS and XPS spectra as shown in Figure 3b,c and Figure 4a, the results present that the sample contains C, O, and I elements after HI acid reduction, and the C/O atomic ratio is increased to above 5, which is more than twice the value of GOPs. The removal of the oxygen-containing groups in the reduction process also can be proved by the high resolution C 1s peaks. As the C 1s spectrum of the GOP shown in Figure 4b, it consists of two main components arising from C−C (~284.8 eV) and C−O (~287 eV) groups and two minor components from C═O (~288.3 eV) and O═C—O (~290.3 eV) groups as earlier reports.[5,9] The C−C bonds become dominant along with the majority of oxygen-containing groups in GO sheets (C−O groups) are almost removed after HI acid reduction (Figure 4c).

Because of the damages on the fine lattice structure of graphene in GO preparation, the r-GOPs have a loose multilayered structure, and their GO sheets could inevitably form curved structures, as shown in Figure 1e. To quantify and compare the alignment degree of the r-GOPs and r-GOP$_{no}$s, we measured the angle-resolved polarized Raman intensity of the sensitive G band, which is widely used in the characterization of arrangement and alignment degree of GO films.[36,37] Figure 5a shows the schematic diagram of the simplified model of GO sheets and the angle-resolved polarized Raman configuration. The laboratory coordinate (x, y, z) is shown in black vectors with the y and z axes parallel and perpendicular to the basal plane/length direction of the r-GOP, respectively. We simplify our models by assuming that the graphene nanosheets of r-GOP are uniformly distributed with an average alignment angle α from the basal plane/length direction. The intensity of a Raman active mode with Raman tensor R_j is calculated by $I = \sum_j |e_s \cdot R_j \cdot e_L|^2$, where e_L and e_s are the unit electric field vectors of the incident laser and scattered Raman signal, respectively. Raman tensors R_j of the G mode can use that of highly oriented pyrolytic graphite (HOPG), and the calculation principle can be found in ref 38. In this work, the incident laser propagates along the x direction and is initially vertically polarized. The laser polarization is then changed continuously through a half-wave plate so that $e_L = (0 \quad \cos\theta \quad -\sin\theta)$ in which θ is the angle between laser polarization and y axis. A polarization analyzer is fixed before the spectrometer to collect only the Raman signal parallel to the y axis with $e_s = (0 \quad 1 \quad 0)$. Therefore, the total Raman intensity of the G mode contributed from both sides of GO films is given by:

$$I_G(\theta) = \frac{1}{2}c^2 \cos^2\alpha\{2 + \cos[2(\alpha - \theta)] + \cos[2(\alpha + \theta)]\} \quad (1)$$

Obviously,I_G would reach the maximum (I_{max}) and minimum (I_{min}) when the electric field vector of the incident laser $e_L$is parallel ($\theta = 0$ and 180°) and perpendicular ($\theta = 90$ and 270°) to the basal plane of the GO films, respectively. Their ratio $I_{max}/I_{min} = \cot^2\alpha$ is monotonically decreasing with α and thus can intuitively quantify their alignment degree. Therefore, the angle-resolved polarized Raman technique can be utilized to compare the alignment degree of the samples we prepared.

The experimental results of r-GOPs and r-GOP$_{no}$s are shown in Figure 5b, the angle (θ) between the electric field vector of the incident laser and the basal plane was tuned from 0 to 350° with a step of 10°. The intensity of the G mode, $I_G(\theta)$, reached a maximum (I_{max}) when the electric field vector of the incident laser was parallel to the basal plane of the r-GOPs and r-GOP$_{no}$s and a minimum (I_{min}) when perpendicular to the basal plane. The result of fitting the experimental data by the eq 1 is indicated by red and blue solid lines in Figure 5b, which is in good agreement with the experimental results. For both r-GOPs and r-GOP$_{no}$s, the experimental I_G (θ) decreases gradually when θ varies from 0 to 90°. From the results shown in Figure 5b, the I_{max}/I_{min} is 8.09 in r-GOP, which corresponds to the averaged alignment angle to be 19.4°. However, the I_{max}/I_{min} is decreased

DOI: 10.1021/acsami.8b19811
ACS Appl. Mater. Interfaces 2019, 11, 10810−10817

to 3.69 in r-GOP$_{no}$s, which corresponds to a larger angle of 27.5°, where that value is slightly smaller than the earlier report[37] in which an averaged alignment angle is 28.3° of GO films fabricated by the flow-directed filtration method. These above results indicate that microstructural evolution occurred and caused improved alignments during the fabrication process by the improved electrospray deposition technique with a moving stage in this work.

The properties of materials are closely related to the internal microstructure. Hence, we infer that the properties of r-GOP based on highly vertically aligned reduced graphene oxide sheets should have advantages in some respect such as electrical conductivity. To verify this, the $I-V$ characteristic of the r-GOP under different temperatures has been measured and displayed in Figure 6. The $I-V$ curves can be well understood by a

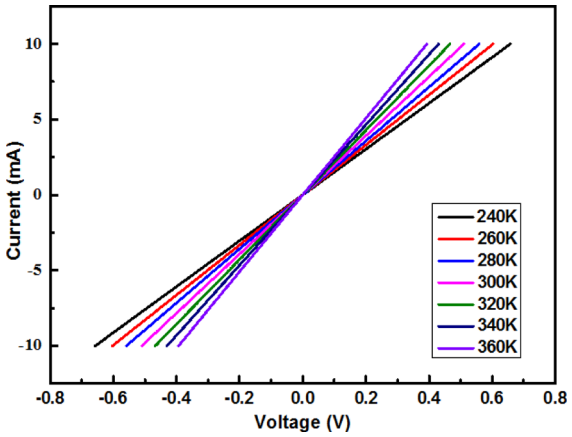

Figure 6. $I-V$ curves at different temperatures of r-GOP.

semiconductor behavior, as the resistance increased with decreasing temperature. To compare the difference of the two kinds of samples, which were fabricated by using the ESD method with or without moving stage used the same usage amount of GO dispersion, the C/O atomic ratios, the I_D/I_G ratios, film thickness, and volume conductivity were listed in Table 1. It can be seen that the C/O atomic ratios and the I_D/I_G ratios of the six samples are almost identical, which indicate that the reduced GO sheets that formed the r-GOPs have the same fundamental qualities. The thickness of r-GOPs is increased in proportion to the usage amount of GO dispersion. Interestingly, the thickness of r-GOPs is always smaller than that of r-GOP$_{no}$s under the same usage amount of GO dispersion, which was caused by the highly vertical alignment of reduced GO sheets in the r-GOPs. This can improve the contact of adjacent reduced GO sheets, which may easier to the electrons to transport in the r-GOP films. As shown in Table 1, the volume conductivities of r-GOPs with different thicknesses have slight variations, but it is far greater than that of r-GOP$_{no}$s.

To further make sure about the favorable characteristics of the r-GOPs, their electrochemical properties were also evaluated on an electrochemical station as the earlier works.[2,39−41,43] In view of the stable structure of the r-GOP films, the symmetrical supercapacitors have been fabricated by using the r-GOP films of different thicknesses (0.7 and 1.2 μm) as the electrodes directly. The CV curves of two thickness electrodes all show well quasi-rectangular shapes at low scan rates, and the shapes were maintained even at a scan rate as high as 200 mV·s^{-1} (Figure 7a,b). This indicates that these two electrodes all show well capacitive properties and have excellent rate capability. GCD tests were also used to study the properties of the thin film electrode. The GCD curves of these two electrodes all show a triangular shape at different current densities (Figure 7c,d), which confirmed by the earlier reports.[1,2] In addition, the tiny voltage drop at the beginning of discharge for all electrodes indicates that the two r-GOP supercapacitors all have small internal charge transfer resistance and solution resistance.[1,2,43]

Furthermore, the specific capacitances were obtained from GCD measurements as the earlier reports.[1] More importantly, the specific capacitances of the 0.7 and 1.2 μm thicknesses of r-GOP were up to 235 and 174 F·g^{-1} at 1 A·g^{-1} (Figure 8a), respectively. They were much larger than that of other graphene paper electrodes, which fabricated by other methods.[2,39−41] The capacitances all drop slowly with further increase of the discharge rate, and the high specific capacitances were still maintained even at a fast discharge rate of 10 A·g^{-1}. These results indicate that the two different thickness r-GOP electrodes all have excellent rate capability. The cyclic performance of the r-GOP electrodes was checked by the GCD cycling test at a current density of 1 A·g^{-1}, which is another key factor for supercapacitors. For the thicker electrode, about 86% of the initial capacitance was retained after 1000 cycles (Figure 8b), which indicate that it has excellent cycling stability. However, this is only about 70% of the thinner electrode. Such a case is most likely due to the poor mechanical performance of the thinner r-GOP films where it is easy to damage an electrode in the process of assembling the supercapacitor.

3. CONCLUSIONS

In conclusion, we report an effective and simple method to prepare vertically aligned GOPs from GO suspensions by using an improved ESD_spr technique with a moving stage, which is controlled by computer. After reduction by using HI acid, the r-GOPs with high integrity and good flexibility were successfully synthesized. The obtained r-GOP has an electrical conductivity

Table 1. Properties Comparison of Six Different Kinds of r-GOPs

samples	fabrication method	reductant	C/O atomic ratio (EDS/XPS)	I_D/I_G	the usage amount of GO dispersion (mL)/thickness of film (μm)	R_s (Ω/sq)	σ (S/m)
r-GOP$_{-1}$	ESD with moving stage	HI	5.60/5.36	1.10	5/0.70 = 7.1	231	6180
r-GOP$_{-2}$	ESD with moving stage	HI	5.63/5.28	1.08	10/1.20 = 8.3	140	5950
r-GOP$_{-3}$	ESD with moving stage	HI	5.57/5.23	1.02	20/2.65 = 7.5	65	5805
r-GOP$_{no-1}$	ESD without moving stage	HI	5.63/5.32	1.18	5/0.87 = 5.7	298	3857
r-GOP$_{no-2}$	ESD without moving stage	HI	5.73/5.11	1.05	10/1.69 = 5.9	151	3918
r-GOP$_{no-3}$	ESD without moving stage	HI	5.59/5.40	1.21	20/3.13 = 6.4	87	3672

DOI: 10.1021/acsami.8b19811
ACS Appl. Mater. Interfaces 2019, 11, 10810−10817

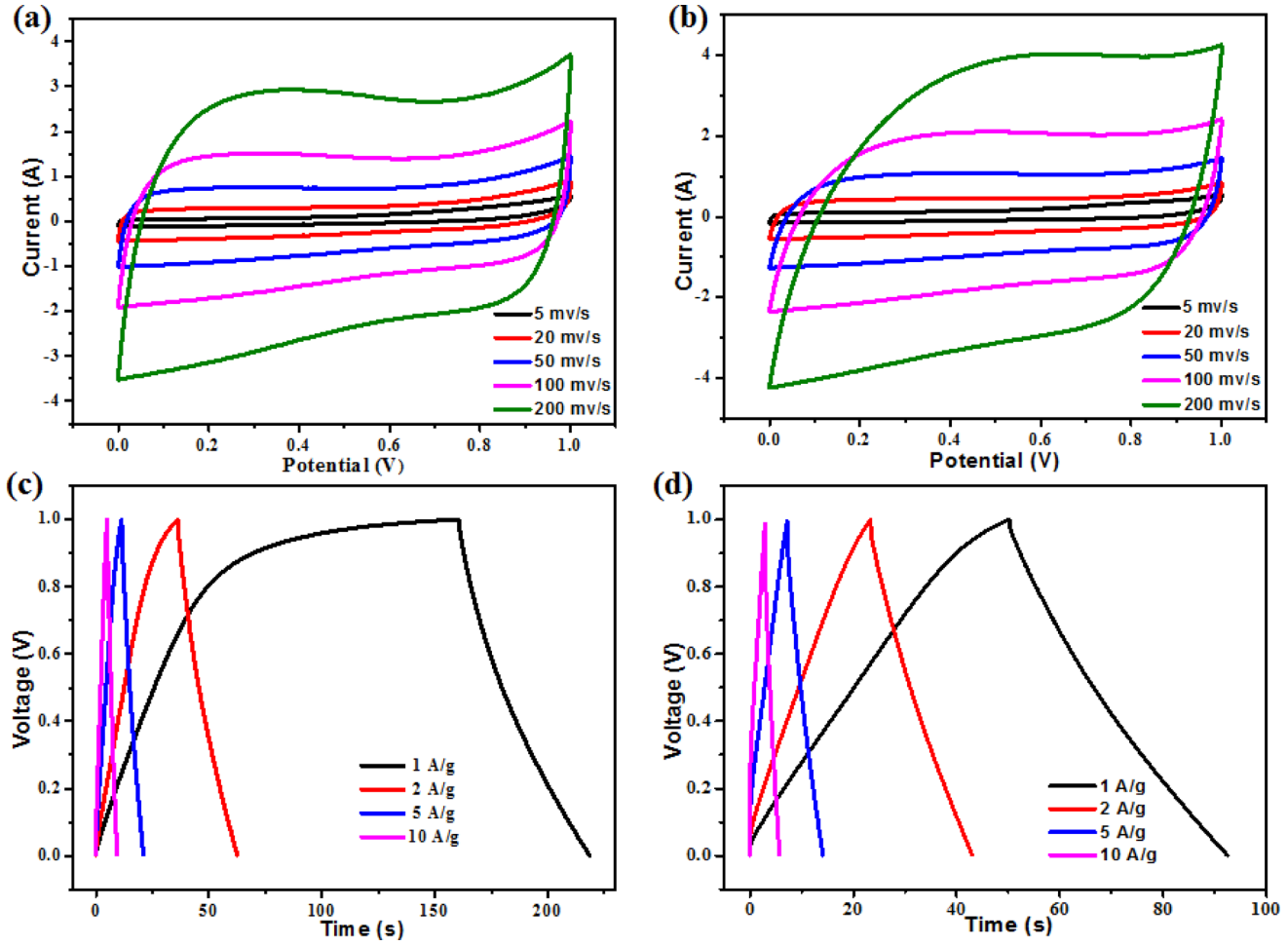

Figure 7. Cyclic voltammetry curves recorded in 6 M KOH of r-GOP electrodes at different scan rates: (a) 0.7 μm thick electrode and (b) 1.2 μm thick electrode. The galvanostatic charge/discharged curves of r-GOP electrodes at different current densities: (c) 0.7 μm thick electrode and (d) 1.2 μm thick electrode.

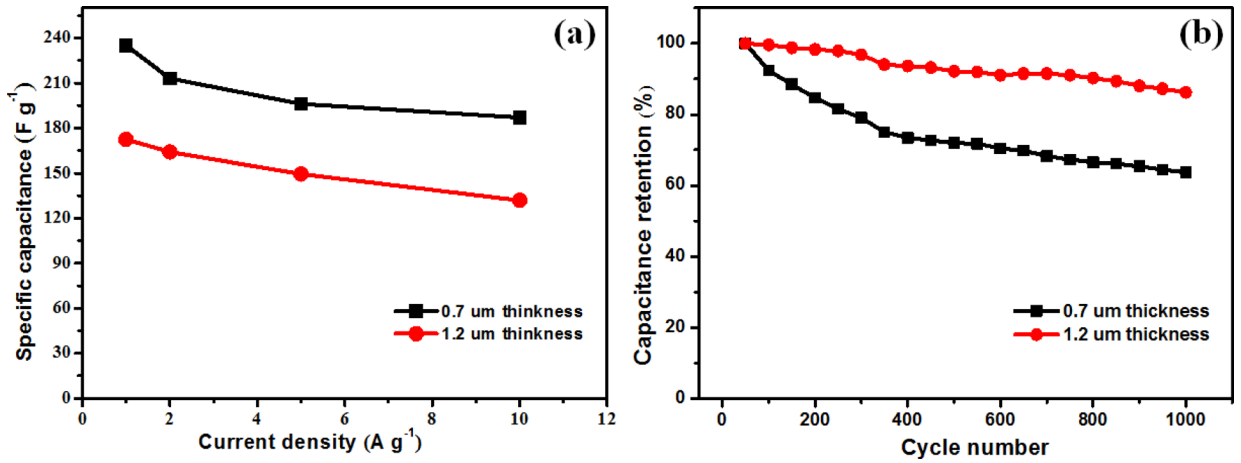

Figure 8. (a) Specific capacitances obtained from GCD measurements as a function of current densities. (b) The capacitance retention of r-GOPs as a function of cycling number.

as high as 6180 S/m, which is more than one and a half times of the r-GOP film, which was fabricated by using the ESD_spr technique without a moving stage. The experimental results approved for the first time that the arrangement and degree of alignment of r-GO sheets can affect the conductivity of the r-GOPs. Further electrochemical measurements for a symmetrical supercapacitor device based on the prepared r-GOP films indicate that it has great capacitive performance and electrochemical stability. It exhibited a relatively high specific capacitance (174 F·g^{-1}) at a current density of 1 A·g^{-1} in 6 M KOH aqueous solution, and its capacitance can retain approximately 86% after 1000 cycles. In addition, patterned

DOI: 10.1021/acsami.8b19811
ACS Appl. Mater. Interfaces 2019, 11, 10810−10817

freestanding r-GOPs, which have potential applications in many fields such as stretchable electronics and wearable devices, also can be fabricated by using this method.

4. EXPERIMENTAL SECTION

4.1. Fabrication of the GOPs. The ESD setup used in this work is schematically showed in Figure S1a. For fabricating the GOP films, the purchased single layer GO dispersion without any further treatment was fed into the needle by a syringe pump at a feeding rate of 30 $\mu L \cdot min^{-1}$, and a voltage of 8 kV was applied between the needle and the polyamide nanofiber film/aluminum foil double-layer substrate (more details are included in Supporting Information), which was place on the two dimensional moving platform. The distance between nozzle and substrate was set as 2.5 cm, and a moving speed of the platform was set to 10 $cm \cdot s^{-1}$. The motion trail of $X-Y$ axis is controlled by running the command program as shown in Figure S1b, and the X axis moving distance was set as 0.5 cm. After the deposition, the GOP films that achieve the expected thickness by adjusting the deposited times on the double-layer substrate were obtained as shown schematically in Figure S2a. To get free-standing GOPs, the polyamide nanofiber film of the double-layer substrate was dissolved by formic acid solution. Thus, the GOP was separated from the aluminum foil. Then, we took out of the aluminum foil and sucked out the formic acid by using a dropper as shown schematically in Figure S2b–d.

4.2. Fabrication of the r-GOPs. As shown in Figure S2e,f, the reduction process was performed by immersing GOP into an HI acid solution and was heated at 100 °C for 1 h. Then, the r-GOP film was washed with deionized water for several times. In the next step as shown schematically in Figure S2f–i, the r-GOP film was salvaged by a Teflon film to avoid the r-GOP film shrinking caused by the surface tension of the deionized water. Afterward, the r-GOP on the Teflon film was put in a draught drying cabinet at 60 °C for 4 h and then could be readily peeled off from a Teflon film because of the interfacial adhesion between them.

4.3. Fabrication of the r-GOP$_{no}$s. For comparison, another reduced graphene oxide paper labeled as r-GOP$_{no}$ was fabricated also by the aforementioned method, and the only difference is keeping the collector substrate still in the ESD process.

■ ASSOCIATED CONTENT

Supporting Information

The Supporting Information is available free of charge on the ACS Publications website at DOI: 10.1021/acsami.8b19811.

The detailed experimental materials and methods, the diagram of the electrospray/electrospinning system, the schematic illustration of preparation procedures of r-GOP, and the Raman spectra of GOP and r-GOP (PDF)

■ AUTHOR INFORMATION

Corresponding Authors

*E-mail: han_wenpeng@163.com (W.-P.H.).
*E-mail: liuxuelu@semi.ac.cn (X.-L.L.).

ORCID

Ping-Heng Tan: 0000-0001-6575-1516
Yun-Ze Long: 0000-0002-4278-4515
Wen-Peng Han: 0000-0003-2540-5832

Notes

The authors declare no competing financial interest.

■ ACKNOWLEDGMENTS

The authors acknowledge support from National Natural Science Foundation of China (11604173, 51673103, and 11474277), Project of Shandong Province Higher Educational Science and Technology Program (J16LJ07), Project funded by China Postdoctoral Science Foundation (2017M612195), Program of Science and Technology in Qingdao City (15-9-1-112-jch), and Natural Science Foundation of Shandong Province, China (BS2015CL013), and P.-H.T. acknowledges support from the Beijing Municipal Science and Technology Commission.

■ REFERENCES

(1) Tang, H.; Yang, C.; Lin, Z.; Yang, Q.; Kang, F.; Wong, C. P. Electrospray-deposition of graphene electrodes: a simple technique to build high-performance supercapacitors. *Nanoscale* **2015**, *7*, 9133–9139.

(2) Beidaghi, M.; Wang, Z.; Gu, L.; Wang, C. Electrostatic spray deposition of graphene nanoplatelets for high-power thin-film supercapacitor electrodes. *J. Solid State Electrochem.* **2012**, *16*, 3341–3348.

(3) Ye, X.; Zhu, Y.; Tang, Z.; Wan, Z.; Jia, C. In-situ chemical reduction produced graphene paper for flexible supercapacitors with impressive capacitive performance. *J. Power Sources* **2017**, *360*, 48–58.

(4) Becerril, H. A.; Mao, J.; Liu, Z.; Stoltenberg, R. M.; Bao, Z.; Chen, Y. Evaluation of solution-processed reduced graphene oxide films as transparent conductors. *ACS Nano* **2008**, *2*, 463–470.

(5) Shin, H.-J.; Kim, K. K.; Benayad, A.; Yoon, S.-M.; Park, H. K.; Jung, I.-S.; Jin, M. H.; Jeong, H.-K.; Kim, J. M.; Choi, J.-Y.; Lee, Y. H. Efficient reduction of graphite oxide by sodium borohydride and its effect on electrical conductance. *Adv. Funct. Mater.* **2009**, *19*, 1987–1992.

(6) Robinson, J. T.; Perkins, F. K.; Snow, E. S.; Wei, Z.; Sheehan, P. E. Reduced graphene oxide molecular sensors. *Nano Lett.* **2008**, *8*, 3137–3140.

(7) Dikin, D. A.; Stankovich, S.; Zimney, E. J.; Piner, R. D.; Dommett, G. H.; Evmenenko, G.; Nguyen, S. T.; Ruoff, R. S. Preparation and characterization of graphene oxide paper. *Nature* **2007**, *448*, 457.

(8) Eda, G.; Fanchini, G.; Chhowalla, M. Large-area ultrathin films of reduced graphene oxide as a transparent and flexible electronic material. *Nat. Nanotechnol.* **2008**, *3*, 270.

(9) Pei, S.; Zhao, J.; Du, J.; Ren, W.; Cheng, H.-M. Direct reduction of graphene oxide films into highly conductive and flexible graphene films by hydrohalic acids. *Carbon* **2010**, *48*, 4466–4474.

(10) Wang, X.; Zhi, L.; Müllen, K. Transparent, conductive graphene electrodes for dye-sensitized solar cells. *Nano Lett.* **2008**, *8*, 323–327.

(11) Liu, Z.; Li, Z.; Xu, Z.; Xia, Z.; Hu, X.; Kou, L.; Peng, L.; Wei, Y.; Gao, C. Wet-spun continuous graphene films. *Chem. Mater.* **2014**, *26*, 6786–6795.

(12) Zhang, M.; Wang, Y.; Huang, L.; Xu, Z.; Li, C.; Shi, G. Multifunctional pristine chemically modified graphene films as strong as stainless steel. *Adv. Mater.* **2015**, *27*, 6708–6713.

(13) Ye, X.; Zhou, Q.; Jia, C.; Tang, Z.; Zhu, Y.; Wan, Z. Producing large-area, foldable graphene paper from graphite oxide suspensions by in-situ chemical reduction process. *Carbon* **2017**, *114*, 424–434.

(14) Guo, Y.; Dun, C.; Xu, J.; Mu, J.; Li, P.; Gu, L.; Hou, C.; Hewitt, C. A.; Zhang, Q.; Li, Y.; Carroll, D. L.; Wang, H. Ultrathin, Washable, and Large-Area Graphene Papers for Personal Thermal Management. *Small* **2017**, *13*, 1702645.

(15) Boukhvalov, D. W.; Katsnelson, M. I. Modeling of graphite oxide. *J. Am. Chem. Soc.* **2008**, *130*, 10697–10701.

(16) Mkhoyan, K. A.; Contryman, A. W.; Silcox, J.; Stewart, D. A.; Eda, G.; Mattevi, C.; Miller, S.; Chhowalla, M. Atomic and electronic structure of graphene-oxide. *Nano Lett.* **2009**, *9*, 1058–1063.

(17) Dong, L.; Hu, C.; Song, L.; Huang, X.; Chen, N.; Qu, L. A Large-Area, Flexible, and Flame-Retardant Graphene Paper. *Adv. Funct. Mater.* **2016**, *26*, 1470–1476.

(18) Fan, X.; Peng, W.; Li, Y.; Li, X.; Wang, S.; Zhang, G.; Zhang, F. Deoxygenation of exfoliated graphite oxide under alkaline conditions: a green route to graphene preparation. *Adv. Mater.* **2008**, *20*, 4490–4493.

(19) Moon, I. K.; Lee, J.; Ruoff, R. S.; Lee, H. Reduced graphene oxide by chemical graphitization. *Nat. Commun.* **2010**, *1*, 73.

(20) Liu, H.; Wang, H.; Zhang, X. Facile fabrication of freestanding ultrathin reduced graphene oxide membranes for water purification. *Adv. Mater.* **2015**, *27*, 249–254.

DOI: 10.1021/acsami.8b19811
ACS Appl. Mater. Interfaces 2019, 11, 10810–10817

(21) Hwang, T. H.; Lee, Y. M.; Kong, B.-S.; Seo, J.-S.; Choi, J. W. Electrospun core−shell fibers for robust silicon nanoparticle-based lithium ion battery anodes. *Nano Lett.* **2012**, *12*, 802−807.
(22) Wu, H.; Zheng, G.; Liu, N.; Carney, T. J.; Yang, Y.; Cui, Y. Engineering empty space between Si nanoparticles for lithium-ion battery anodes. *Nano Lett.* **2012**, *12*, 904−909.
(23) Zhu, Y.; Han, X.; Xu, Y.; Liu, Y.; Zheng, S.; Xu, K.; Hu, L.; Wang, C. Electrospun Sb/C fibers for a stable and fast sodium-ion battery anode. *ACS Nano* **2013**, *7*, 6378−6386.
(24) Li, Y.; Guo, B.; Ji, L.; Lin, Z.; Xu, G.; Liang, Y.; Zhang, S.; Toprakci, O.; Hu, Y.; Alcoutlabi, M.; Zhang, X. Structure control and performance improvement of carbon nanofibers containing a dispersion of silicon nanoparticles for energy storage. *Carbon* **2013**, *51*, 185−194.
(25) Liu, Y.; Yu, S.; Feng, R.; Bernard, A.; Liu, Y.; Zhang, Y.; Duan, H.; Shang, W.; Tao, P.; Song, C.; Deng, T. A bioinspired, reusable, paper-based system for high-performance large-scale evaporation. *Adv. Mater.* **2015**, *27*, 2768−2774.
(26) Mustafa, M.; Awais, M. N.; Pooniah, G.; Choi, K. H.; Ko, J.; Doh, Y. H. Electrospray deposition of a graphene-oxide thin film, its characterization and investigation of its resistive switching performance. *J. Korean Phys. Soc.* **2012**, *61*, 470−475.
(27) Xin, G.; Sun, H.; Hu, T.; Fard, H. R.; Sun, X.; Koratkar, N.; Borca-Tasciuc, T.; Lian, J. Large-Area Freestanding Graphene Paper for Superior Thermal Management. *Adv. Mater.* **2014**, *26*, 4521−4526.
(28) Varea, A.; Monereo, O.; Xuriguera, E.; Prades, J. D.; Cirera, A. Electrospray as a suitable technique for manufacturing carbon-based devices. *J. Phys. D: Appl. Phys.* **2017**, *50*, 315301.
(29) Sun, B.; Long, Y.-Z.; Liu, S.-L.; Huang, Y.-Y.; Ma, J.; Zhang, H.-D.; Shen, G.; Xu, S. Fabrication of curled conducting polymer microfibrous arrays via a novel electrospinning method for stretchable strain sensors. *Nanoscale* **2013**, *5*, 7041−7045.
(30) Terao, T.; Zhi, C.; Bando, Y.; Mitome, M.; Tang, C.; Golberg, D. Alignment of boron nitride nanotubes in polymeric composite films for thermal conductivity improvement. *J. Phys. Chem. C* **2010**, *114*, 4340−4344.
(31) Vallés, C.; Núñez, J. D.; Benito, A. M.; Maser, W. K. Flexible conductive graphene paper obtained by direct and gentle annealing of graphene oxide paper. *Carbon* **2012**, *50*, 835−844.
(32) Park, S. M.; Kim, D. S. Electrolyte-Assisted Electrospinning for a Self-Assembled, Free-Standing Nanofiber Membrane on a Curved Surface. *Adv. Mater.* **2015**, *27*, 1682−1687.
(33) Yu, G.-F.; Yan, X.; Yu, M.; Jia, M.-Y.; Pan, W.; He, X.-X.; Han, W.-P.; Zhang, Z.-M.; Yu, L.-M.; Long, Y.-Z. Patterned, highly stretchable and conductive nanofibrous PANI/PVDF strain sensors based on electrospinning and in situ polymerization. *Nanoscale* **2016**, *8*, 2944−2950.
(34) Stankovich, S.; Dikin, D. A.; Piner, R. D.; Kohlhaas, K. A.; Kleinhammes, A.; Jia, Y.; Wu, Y.; Nguyen, S. T.; Ruoff, R. S. Synthesis of graphene-based nanosheets via chemical reduction of exfoliated graphite oxide. *Carbon* **2007**, *45*, 1558−1565.
(35) Wu, J.-B.; Lin, M.-L.; Cong, X.; Liu, H.-N.; Tan, P.-H. Raman spectroscopy of graphene-based materials and its applications in related devices. *Chem. Soc. Rev.* **2018**, *47*, 1822−1873.
(36) Liang, Q.; Yao, X.; Wang, W.; Liu, Y.; Wong, C. P. A Three-Dimensional Vertically Aligned Functionalized Multilayer Graphene Architecture: An Approach for Graphene-Based Thermal Interfacial Materials. *ACS Nano* **2011**, *5*, 2392−2401.
(37) Dai, Z.; Wang, Y.; Liu, L.; Liu, X.; Tan, P.; Xu, Z.; Kuang, J.; Liu, Q.; Lou, J.; Zhang, Z. Hierarchical Graphene-Based Films with Dynamic Self-Stiffening for Biomimetic Artificial Muscle. *Adv. Funct. Mater.* **2016**, *26*, 7003−7010.
(38) Liu, X.-L.; Zhang, X.; Lin, M.-L.; Tan, P.-H. Different angle-resolved polarization configurations of Raman spectroscopy: A case on the basal and edge plane of two-dimensional materials. *Chin. Phys. B* **2017**, *26*, 067802.
(39) Le, L. T.; Ervin, M. H.; Qiu, H.; Fuchs, B. E.; Lee, W. Y. Graphene supercapacitor electrodes fabricated by inkjet printing and thermal reduction of graphene oxide. *Electrochem. Commun.* **2011**, *13*, 355−358.
(40) Shi, W.; Zhu, J.; Sim, D. H.; Tay, Y. Y.; Lu, Z.; Zhang, X.; Sharma, Y.; Srinivasan, M.; Zhang, H.; Hng, H. H.; Yan, Q. Achieving high specific charge capacitances in Fe_3O_4/reduced graphene oxide nanocomposites. *J. Mater. Chem.* **2011**, *21*, 3422−3427.
(41) Wang, G.; Sun, X.; Lu, F.; Sun, H.; Yu, M.; Jiang, W.; Liu, C.; Lian, J. Flexible pillared graphene-paper electrodes for high-performance electrochemical supercapacitors. *Small* **2012**, *8*, 452−459.
(42) Alzate-Carvajal, N.; Acevedo-Guzmán, D. A.; Meza-Laguna, V.; Farías, M. H.; Pérez-Rey, L. A.; Abarca-Morales, E.; García-Ramírez, V. A.; Basiuk, V. A.; Basiuk, E. V. One-step nondestructive functionalization of graphene oxide paper with amines. *RSC Adv.* **2018**, *8*, 15253−15265.
(43) Chaitoglou, S.; Amade, R.; Bertran, E. Evaluation of graphene/WO_3 and graphene/CeO_x structures as electrodes for supercapacitor applications. *Nanoscale Res. Lett.* **2017**, *12*, 635.

DOI: 10.1021/acsami.8b19811
ACS Appl. Mater. Interfaces 2019, 11, 10810−10817